Journal of
NANOSTRUCTURES
JNS
NANOSTRUCTURES
JNS.kashanu.ac.ir

Facile Fabrication of Boron-Doped Titania Nanopowders by Atmospheric Pressure Chemical Vapor Synthesis Route and its Photocatalytic Activity

K. Saberyan [a]*, N.S. Mazhari [b], M. Rahiminezhad-Soltani [c], M.A. Mohsen [d]

[a] *Fuel Cycle Research School, NSTRI, P.O. Box: 11365–8486, Tehran, Iran.*

[b] *Physics and Nuclear Engineering Faculty, Amirkabir University , P.O. Box: 15875–4413, Tehran, Iran.*

[c] *Young Researchers and Elite Club, Saveh Branch, Islamic Azad University, P. O. Box: 39187–366, Saveh, Iran.*

[d] *Radiation Applications Research School, NSTRI, P.O.Box: 14395-836, Tehran, Iran.*

Article history:
Received 12/3/2014
Accepted 17/5/2014
Published online 1/6/2014

Keywords:
Atmospheric pressure
Chemical vapor Synthesis
B-doped Titania
TiO_2 nanoparticles
Boron
CVS

**Corresponding author:*
E-mail address:
saberyan@aeoi.org.ir
Phone: +98 21 82062536
Fax: +98 21 88221128

Abstract

The Atmospheric Pressure Chemical Vapor Synthesis (APCVS) route is a process that can be used for the synthesis of doped-nanocrystalline powders with very small crystallite sizes having a narrow particle size distribution and high purity. In this study, APCVS technique was used to prepare boron-doped titania nanopowders. The effects of temperature, borate flow rate and water flow rate on the amount of doped boron were studied. The resultant powders were characterized by inductively coupled plasma (ICP), X-ray diffraction (XRD), nitrogen adsorption technique (BET), UV-visible DRS spectroscopy, scanning electron microscopy (SEM), and transmission electron microscopy (TEM). The optimum boron precursor flow rate was 80 sccm. The highest amount of doped boron was attained when water flow rate was 900 sccm. In comparison to the pristine TiO_2, the boron-doped TiO_2 nanoparticles showed blue-shift in band-gap energy of the samples.

1. Introduction

Nowadays there is a good interest to utilize doped nanoparticles due to their application in solar cells [1], gas sensors [2], self-cleaning coatings [3, 4], magnetic, optical and electrical applications [5], removing environmental pollutants [6], and etc. Among different semiconductors, TiO_2 have achieved high attention due to high oxidation power, low cost, abundance, non toxicity, and high chemical stability [7-9]. TiO_2 has three famous structure consisted of anatase, rutile, brookite and a rather newcomer phase, TiO_2 (B) [4, 8, 10]. Between these, anatase and rutile are more applicable and the anatase phase shows a higher photocatalytic activity [7]. However, its application is limited due to wide band gap (3.2 eV and 3.0 eV for anatase and rutile), causing activity only under UV irradiation

[4, 7, 8, 11, 12]. Therefore many researchers are investigating on decreasing the band gap by metal ion implantation, doping with anions, transition metals and rare earth metals and metalloids by different methods such as sol-gel, hydrothermal, laser pyrolysis, chemical vapor deposition (CVD), chemical vapor synthesis (CVS), etc [3, 5-9, 11-17]. CVS is a facile and useful process due to its high purity, unagglomeration, high flexibility in using different kind of precursors and well controlled conditions. CVS process can be used in atmospheric pressure (APCVS), so it doesn't need expensive vacuum instruments [10, 18]. In our study, boron doped TiO_2 were synthesized via CVS method in presence of H_2O and were characterized by several analyses.

2. Experimental procedure

2.1. Nanopowder synthesis

The system configuration used in this experiment is shown in figure 1, schematically. Purified argon (Ar, purity >99.999%) carrier gas is divided to four parts. These parts are blown into bubblers containing $TiCl_4$ (purity >99.999% MERCK) as TiO_2 precursor, trimethyl borate ($C_3H_9BO_3$) as boron precursor, purified water and other as pure Ar to fix the total flow rate. Additional oxygen (purity >99.999%) is mixed to these to ensure $TiCl_4$ complete reaction. The mixture is introduced to a hot-wall tubular quartz reactor with 8 cm-in diameter and 80 cm length that is heated by an external resistance furnace. The effective heated region is 20 cm in the middle of quartz reactor. The products are collected at the end of tube through two ways simultaneously, as powder through cooling by fan that particles are settled down on tube's wall and as solution through entering those particles which didn't trapped as powder with exhaust gases in a bubbler. Total flow rate and pressure are 2.1 liter per minute and 1 bar in all of processes respectively. The volume of introduced precursors and gases are controlled by needle valves and flow meters and gases pressure is controlled by pressure indicator.

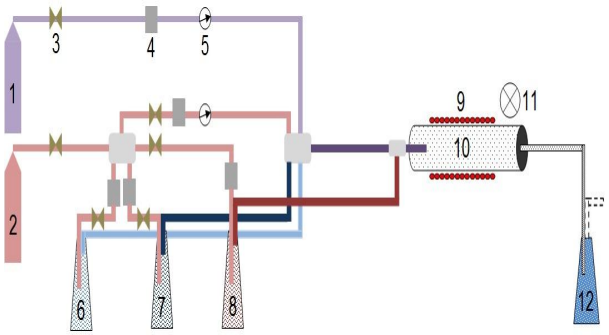

Fig. 1. Schematic diagram of CVS configuration. 1) Oxygen, 2) Argon, 3) needle valve, 4) flow meter, 5)pressure indicator, 6) water, 7) trimethyl borate, 8) $TiCl_4$, 9) furnace, 10) quartz tube, 11) cooling fan, 12) collected particles.

Oxygen, Titanium tetrachloride ($TiCl_4$), and purified water were used as starting materials and introduced to the reactor in 500, 500 and 900 sccm flow rate respectively. Trimethyl borate ($C_3H_9BO_3$) was introduced as boron precursor in 20, 40, 60, 80, and 100 sccm and reactor temperature was determined 400°C.

Different reaction temperatures and its effects were studied in the next step. Reactor temperature was changed in 400, 600, 700, 800, and 900°C and precursors were in the room temperature. Oxygen, $TiCl_4$, water, and trimethyl borate were introduced to the reactor in 500, 500, 900 and 80 sccm flow rate respectively. These experiments were carried out to investigate the effect of boron on the photocatalytic activity of TiO_2 nanopowders and the effects of temperature, water flow rate and Boron precursor on the B-doped TiO_2 properties respectively. Scanning electron microscopy (SEM) (KYKY- EM3200- 25kV), transmission electron microscopy (TEM) (Philips- EM- 208S- 100kV),

induced coupled plasma (ICP) (Perklin Emler-Optima 2000 DV), X-ray diffraction (XRD) (Stoe-Stidy-MP), nitrogen adsorption technique (BET) (QUANTACHROME- Nova 2000), and UV-visible DRS (Shimadzu- MPC-2200) were used to characterize the final products.

2.2 Measuring the amount of doped boron

The amount of boron incorporated in the B-doped TiO_2 was measured by inductively coupled plasma (ICP). For this measurement, B-doped TiO_2 powders were dissolved in a mixture of nitric acid and fluoric acid at a molar ratio of 4:1 [7] and were heated for 24 hours.

3. Results and discussion

3.1. Effect of temperature on amount of doped boron

Table 1 shows the changes in amount of doped boron with synthesis temperature. As it's shown in table 1 the amount of boron was decreased when temperature was increased to 800°C and again was increased when temperature was 900°C. At 400 °C the powder was white, when temperature was increased to 600°C, color of powder was changed to gray and it was converted to white gradually, till to 900°C. Water flow rate and trimethyl borate flow rate were 900 and 80 sccm respectively.

Table 1. Amount of doped boron in terms of synthesis temperature

Temperature (°C)	Amount of doped boron (ppm)
600	224.9
700	122.5
800	79.4
900	259.4

3.1.1. XRD

XRD patterns were determined the structure of B-doped TiO_2 in different reaction temperatures and its result is shown in figure 2. The peaks for the (1 0 1), (0 0 4), (2 0 0), (1 0 5), and (2 1 1) reflections characteristic of the TiO_2 anatase phase appeared. Process temperatures ranging from 600 to 900°C produce the anatase phase. The intensity of peaks was been sharper, increasing temperature.

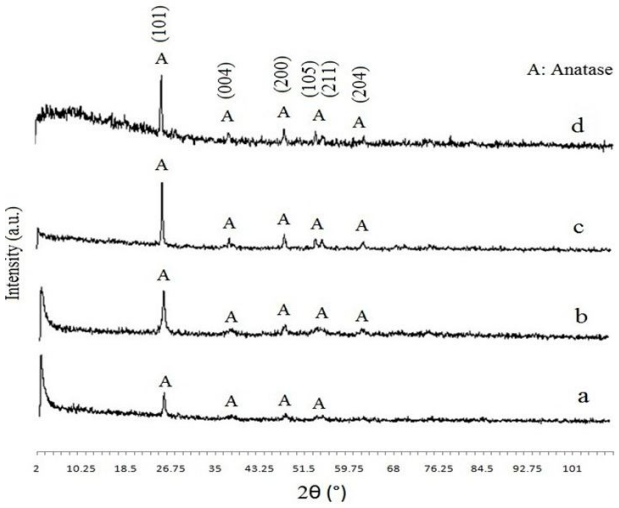

Fig. 2. X-ray diffraction pattern of B-doped TiO_2 under different reaction temperature. a)600°C, b)700°C, c)800°C, d)900°C.

However amorphous phase was appeared in 900°C. Therefore, it was strongly suggested the synthesis temperature should not exceed 900°C due to the appearance of the amorphous phase. It's noticeable that there is no indication of rutile peaks in the pattern even in 900°C .The diffraction peaks for boron or boron containing phases were not observed, which indicated that boron was highly dispersed on TiO_2, or XRD was not sensitive enough to detect such minor changes to TiO_2.

Also the average crystalline size was calculated by the Scherrer relationship, using XRD results:

$$d_{XRD} = 0.9\,\lambda / \beta \cos\theta \qquad (1)$$

Where λ is the wavelength of the incident x-ray, θ the Bragg angle and β the full width at half

maximum (FWHM) [21]. As shown in Table 2, the crystalline sizes were increase with increasing the synthesis temperature. Vapor molecule accretion caused the crystalline size of TiO_2 to gradually increase as the temperature increased. Cluster–cluster and particle–particle collided rapidly, accelerating crystalline growth size (primary particle) and cluster (secondary particle).

3.1.2. BET

Table 2 shows the specific surface area of samples analyzed by the BET method. Agglomeration caused the surface area to decrease as the synthesis temperature increased. Furthermore, TEM observation confirmed that the prepared TiO_2 powders had an almost spherical and nonporous form. Therefore, this relationship can be expressed by a simple equation, assuming a spherical and nonporous particle:

$$d_{BET} = 6 / S_{BET}\rho_T \quad (2)$$

where d_{BET} is the calculated particle size (nm), ρ_T is the TiO_2 theoretical density (3.84 g/cm^3 for anatase) [17], and S_{BET} is the specific surface area (m^2/g).

The results of specific surface area agree well with the TEM observation (Fig. 4), but were different from the XRD calculations. Maira and coworkers [22] claim that the specific surface area of sol–gel synthesized TiO_2 depends only on the size of crystals (primary particle) and was unaffected by aggregation. This is probably because aggregation in the sol–gel process is loose, so the N_2 gas can penetrate the gap between aggregated particles. In this study, TiO_2 aggregation occurs mostly at high temperatures (>500 ˚C); therefore, the particles are tightly aggregated with high surface energy. Nakaso and coworkers [23] report this phenomenon as incomplete sintering in the CVS process. Hence, the specific surface area is more related to secondary particles than primary particles in CVS process. Degree of agglomeration (N) was determined by equation (3) [21] and is shown in table 2:

$$N = d^3_{BET} / d^3_{XRD} \quad (3)$$

Table 2. Results of prepared B-doped TiO_2 at different synthesis temperature

Sample	Boron flow rate (sccm)	Water flow rate (sccm)	Temp. (°C)	Boron amount (ppm)	S_{BET} (m^2/g)	d_{XRD} (nm)	d_{BET} (nm)	Degree of Agglomeration N= d^3_{BET} / d^3_{XRD}
1	80	900	600	224	64.71	25	24	0.885
2	80	900	700	122	43.55	50	35	0.343
3	80	900	800	79	61.13	50	25	0.125
4	80	900	900	259	27.05	92	57	0.237

3.1.3. SEM

The SEM micrographs of B-doped TiO_2 nanoparticles are shown in Figure 3. From SEM analysis of the formed TiO_2 at different temperatures, the morphology difference of formed TiO_2 was observed. It was indicated that controlling temperature was critical to the control of size, size distribution and agglomeration of doped TiO_2. The dimensions of the TiO_2 nanoparticles in figure 3 (A - D) ranged from ~20 to ~100 nm and they are in spherical shapes. In addition, the nanoparticles aggregated and formed large particle blocks while increasing temperature.

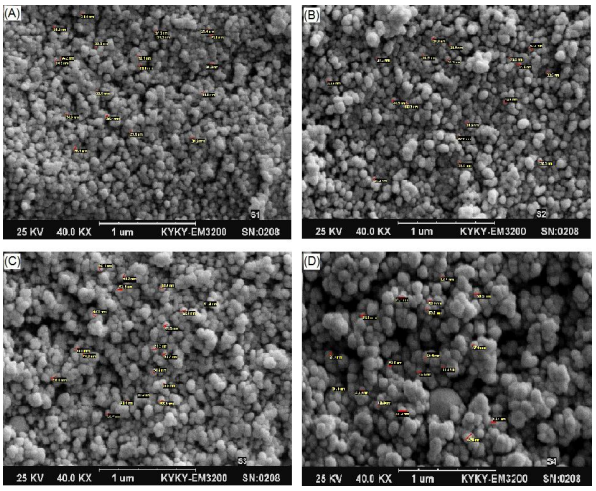

Fig. 3. Boron-doped TiO_2 nanoparticles in different temperatures: A) 600°C, B)700°C, C)800°C, D)900°C.

3.1.4. TEM

TEM was applied to determine particle size, morphology, coagulation and agglomeration. As it is shown in figure 4, TEM observation confirmed that the prepared TiO_2 powders had an almost spherical and nonporous form. The size distribution of particles was narrow and non-aggregated in the lower temperatures of 600 and 700°C. In contrast, the sol–gel nanoparticle preparation method easily produced particle agglomeration after calcinations at high temperatures. The CVS process can produce a good visible-light-responsive TiO_2 without agglomeration under proper conditions. Morphological observations by TEM and XRD reveal that the large particle size of TiO_2 was mainly caused by agglomeration, not the growth of crystallite size.

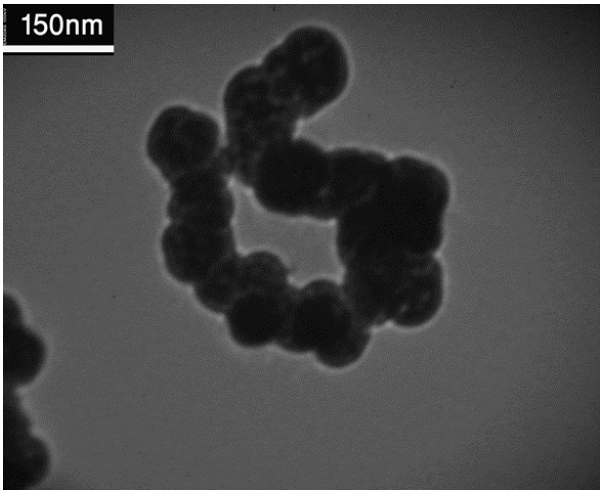

Fig. 4. TEM photograph of B-doped TiO_2.

3.2. Effect of boron precursor flow rate on amount of doped boron

Table 3 shows the changes in amount of doped boron with boron flow rate. As it's shown in table 3, amount of boron in TiO_2 is increased as trimethyl borate flow rate is increased to 80 sccm, and its amount is decreased when trimethyl borate flow rate is 100 sccm.

Table 3. Amount of doped boron in terms of trimethyl borate flow rate changes.

trimethyl borate flow rate (sccm)	amount of doped boron(ppm)
20	75.0
40	251.0
60	350.0
80	444.0
100	251.0

It is noteworthy that the temperature and water flow rate were 400°C and 700 sccm respectively.

3.3. Effect of water flow rate on amount of doped boron

Table 4 shows the changes in amount of doped boron with water flow rate. As it's shown in table 4, the highest amount of boron was attained when water flow rate was 900 sccm. It is noteworthy that the temperature and trimethyl borate flow rate were 400°C and 80 sccm respectively.

Table 4. Amount of doped boron in terms of water flow rate changes.

Water Flow Rate (sccm)	Amount of doped Boron (ppm)
700	474.0
900	1361.0
1100	1043.5
1300	608.6

3.4. Effect of boron on light absorption

The ultraviolet–visible light diffuse reflectance spectra (UV–Vis DRS) with a spectrophotometer was used to determine the absorption edge shift of B-doped TiO_2 nanopowder at room temperature in the wavelength range of 200–800 nm and it's results is shown in figure 5 as compared to pure TiO_2. As it is shown in this figure, B-doped TiO_2 shows more absorption in comparison to pure TiO_2 in the UV region. However a shift to UV region in the absorption edge of TiO_2 was seen when B was doped as the absorption edge is changed from 410 nm (pure TiO_2) to 380 nm for B-doped TiO_2. The UV–Vis reflectance band edge depends strongly on TiO_2 particle size, which can be attributed to the quantum size effect of semiconductors [19].

Doping boron obviously affects light absorption characteristics of TiO_2, as shown in Figure 5. It is obvious that B-doped TiO_2 shows higher photocatalytic activity in UV region. Samples prepared in higher temperatures show higher photocatalytic activity, which could be due to the formation of anatase [7].

The absorption onset of each product was determined by a least-squares fit of the linear region of a $(Ah\nu)^2$ vs. hν plot (A= absorbance, h= Planck's constant, and ν= frequency), as presented in Figure 6. Due to the position of their absorption threshold, band gaps of 3.2 eV for pure TiO_2 and 3.4 eV for B-doped TiO_2 were obtained [24].

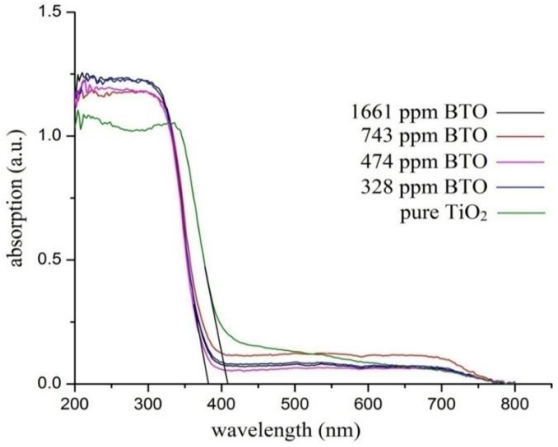

Fig. 5. UV-Visible absorption spectra for prepared doped TiO_2 with different amount of boron in comparison to pure TiO_2.

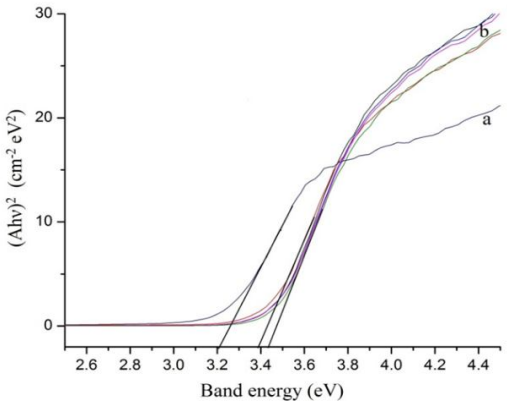

Fig. 6. Plots of $(Ahv)^2$ vs. Band energy for a) pure TiO_2 and b) B-doped TiO_2 nanoparticles.

4. Conclusion

Boron doped nanocrystalline titania powders were synthesized by a one step method using atmospheric pressure chemical vapor synthesis (APCVS). Here, trimethyl borate and $TiCl_4$ were used as a boron and TiO_2 feedstock, respectively. Within a certain range of the growth temperatures the TiO_2 nanoparticles were crystalline and had pure anatase structure. The particle size and crystallinity of the nanoparticles increases with increasing temperature. The nanopowders were showed extended absorption in UV region. In comparison to the pristine TiO_2, the boron-doped TiO_2 nanoparticles showed blue-shift in band-gap energy of the samples.

Acknowledgment

The authors would like to thank the Iranian Nanotechnology Initiative Council (Tehran, Iran) for their kind cooperation.

References

[1] C.-S. Chou, Y.J. Lin, R.Y. Yang, K.H. Liu, Adv. Powder. Technol. 22 (2011) 31-42.

[2] X. Hu, G. Li, and J. C. Yu, Langmuir 26 (2009) 3031-3039.

[3] A. Zaleska, Recent Pat. Eng. 2 (2008) 157-164.

[4] N. S. Allen, M. Edge, J. Verran, J. Stratton, J. Maltby, C. Bygott, Polym. Degrad. Stabil. 93 (2008) 1632-1646.

[5] K. Karthik, S. K. Pandian, N. V. Jaya, Appl. Surf. Sci. 256 (2010) 6829-6833.

[6] C. Chen, H. Bai, S.M. Chang, C. Chang, W. Den, J. Nanopart. Res. (2007) 365-375.

[7] N. Khakpash, A. Simchi, T. Jafari, J. Mater. Sci-Mater. El. 23 (2012) 659-667.

[8] H. Jie, H.B. Lee, K.H. Chae, M.Y. Huh, M. Matsuoka, S.H. Cho, et al., Res. Chem. Intermediat. 38 (2012) 1171-1180.

[9] L. Deng, Y. Chen, M. Yao, S. Wang, B. Zhu, W. Huang, et al. J. Sol-Gel. Sci. Techn. 53 (2010) 535-541.

[10] M. Rahiminezhad-Soltani, K. Saberyan, F. Shahri, A. Simchi, Powder Technol. 209 (2011) 15–24.

[11] I.M. Ahmad, S.S. Bhattacharya, H. Hahn, Process. App. Ceram. 3 (2009) 113-117.

[12] D.B. Hamal, K.J. Klabunde, J. Colloid. Interf. Sci. 311 (2007) 514-522.

[13] M. Wojtoniszak, D. Dolat, A. Morawski, E. Mijowska, Nanoscale. Res. Lett. 7 (2012) 1-6.

[14] Z. Jian-Guo, Z. Wei-Ying, M. Zi-Wei, X. Er-Qing, A.K. Zhao, L. Zhao-Jun, Chinese Phys. B 20 (2011) 087701-087704.

[15] R. Alexandrescu, I. Morjan, M. Scarisoreanu, R. Birjega, C. Fleaca, I. Soare, et al., Infrared Phys. Techn. 53 (2010) 94-102.

[16] E. Setiawati, K. Kawano, J Alloy Compd, 451 (2008) 293-296.

[17] C.-S. Kuo, Y.H. Tseng, C.H. Huang, Y.Y. Li, J. Mol. Catal. A-Chem. 270 (2007) 93-100.

[18] M. T. Swihart, Curr. Opin. Colloid. In. 8 (2003) 127-133.

[19] J. F. Banfield, H. Zhang, Rev. Mineral. Geochem. 44 (2001) 1-58.

[20] N. D. Abazović, D. J. Jovanović, M. M. Stoiljković, M. N. Mitrić, P. S. Ahrenkil, J. M. Nedeljković, et al., J. Serb. Chem. Soc. 77 (2012) 789-797.
[21] K. K. Akurati, S. Bhattacharya, M. Winterer, H. Hahn, J. Phys. D Appl. Phys. 39 (2006) 2248-2254.
[22] A. Maira, K. Yeung, C. Lee, P. Yue, C. Chan, J. Catal. 192 (2000) 185-196.
[23] K. Nakaso, K. Okuyama, M. Shimada, S.E. Pratsinis, Chem. Eng. Sci. 58 (2003) 3327–3335.